Tiny Yet Tough: Maximizing the Toughness of Fiber-Reinforced Soft Composites in the Absence of a Fiber-Fracture Mechanism

Wei Cui,[1] Yiwan Huang,[2] Liang Chen,[3] Yong Zheng,[3] Yoshiyuki Saruwatari,[4] Chung-Yuen Hui,[1,5] Takayuki Kurokawa,[1,2] Daniel R. King,[1,2,*,#] and Jian Ping Gong[1,2,6,*]

[1]Global Station for Soft Matter, Global Institution for Collaborative Research and Education (GI-CoRE), Hokkaido University, Sapporo 001-0021, Japan;

[2]Faculty of Advanced Life Science, Hokkaido University, Sapporo 001-0021, Japan;

[3]Graduate School of Life Science, Hokkaido University, Sapporo 001-0021, Japan;

[4]Osaka Organic Chemical Industry Ltd., Osaka, 541-0052, Japan;

[5]Field of Theoretical & Applied Mechanics, Department of Mechanical & Aerospace Engineering, Cornell University, Ithaca, New York 14853, USA;

[6]Institute for Chemical Reaction Design and Discovery (WPI-ICReDD), Hokkaido University, Sapporo 001-0021, Japan.

Corresponding authors

*(D.R.K.) E-mail: dking@sci.hokudai.ac.jp; Tel & Fax +81-(0)11-706-9012.

*(J.P.G.) E-mail: gong@sci.hokudai.ac.jp; Tel & Fax +81-(0)11-706-9011.

Lead author:

[#](D.R.K.) E-mail: dking@sci.hokudai.ac.jp.

SUMMARY:

The toughness of composite materials is size dependent below a critical load transfer length (l_T) and maximizing the toughness at considerably small length scales is important towards developing robust, size-limited applications. Fiber-reinforced viscoelastic polymers are uniquely qualified to study the size-limited regime because the l_T of these soft composites can be as high as several centimeters, in contrast to traditional composites where l_T is extremely small, allowing a large window for macroscale characterization. In this work, we elucidate the parameters that influence the toughness of soft composites when failure is governed by a fiber-pullout induced matrix-fracture mechanism. Under these conditions, composite toughness (T) follows an empirical relation $T = 0.5 \cdot K \cdot T_m \cdot (w - w_{cc}) + T_m$, where K is the fiber bundle geometry factor, T_m is the matrix toughness, w is the composite width, and w_{cc} is the center-to-center distance between adjacent fiber bundles. Through this work, we demonstrate three important points: 1) fiber-reinforced viscoelastic polymers can possess high toughness even at dimensions well below l_T, 2) significant toughness amplification occurs due to the presence of fibers, even when the fracture process consists solely of matrix rupture, and 3) the composite toughness in the fiber-pullout region can be predicted from easily attainable component parameters.

Keywords: Fiber-reinforced soft composites, toughness amplification, fiber pullout, fracture toughness, size dependence

1. INTRODUCTION

Cutting-edge applications in the fields of soft robotics and advanced medical devices require materials with a combination of small size, high strength, low flexural stiffness, and high crack resistance. Molecular-scale composites, such as double-network materials, hybrid viscoelastic hydrogels, and nanocomposites have shown promise in achieving some of these requirements.[1-6] However, integrating all of these required yet often contradicting properties into one material system is still a daunting challenge.

Soft fiber-reinforced polymers (FRPs) are promising materials due to their unique mechanical and physical properties.[7-14] Traditional soft FRPs are made by laminating or curing rubbery polymers with stiff fabrics, and have found use in large-size structural and load-bearing applications such as flexible aircraft fuel tanks and pneumatic tires.[14, 15] These materials however are often plagued by poor crack resistance due to delamination and interfacial failure. Recently, extraordinarily crack-resistant soft FRPs have been developed by combining strong and stiff fibers with viscoelastic hydrogels or elastomers as matrices, [17-19] exhibiting fracture energy up to 2500 kJ m^{-2}.[21-26] These soft composites show extremely high toughness due to the synergetic effect of three features of the soft matrix: strong bonding to fibers, low modulus (10^4~10^5 orders lower than the fibers), and high work to rupture (comparable to that of the fibers). As a result, these soft composites have a very large load transfer length (l_T), on the centimeter-scale, and high energy dissipation density due to concurrent fracture of the fiber and matrix. We have shown that for a sufficiently large specimen size, $w > l_T$, the tearing energy (toughness) of the soft composites, Γ, is quantitatively related to the volume-weighted average of the work to rupture of the two components, W, and the load transfer length, l_T, as $\Gamma = W \cdot l_T$,[20, 27, 28] where l_T scales with the square root of the fiber/matrix modulus ratio and can be explicitly calculated for a given component combination and geometry.[29, 30] At large size-scales, these materials show extraordinary crack resistance, even

exceeding metals, with significantly reduced weight and low cost.[31, 32]

When the size, w, of these soft composites is decreased below l_T, the toughness decreases from the plateau value and becomes size-dependent due to a change in fracture mechanism (**Figure 1a**).[19, 20] The apparent size dependence in **Figure 1a** can be divided into three regions (**Figure 1b**) according to the failure process. A transition from fiber and matrix concurrent fracture at the saturated toughness (Region III) to a mixed-mode fiber fracture/pullout mechanism (Region II) occurs at $w \approx l_T$. For sufficiently small composites, the failure mechanism consists of only fiber pullout with no fiber fracture (Region I). The width at which this transition occurs is referred to as w_1. Composites with specimen size below l_T are not able to fully utilize the fiber fracture energy dissipation mechanism, resulting in reduced toughness. However, if we compare the toughness of the composites observed in Region I to the neat matrix and fabric, we see that within this region they are still capable of exhibiting toughness much greater than either neat component (**Figure 1c**). The energy dissipation mechanism that governs Region I where only fiber-pullout occurs is currently unknown, yet these composites fulfill many of the complex mechanical requirements for small-scale soft material devices, making them worthy of further study.

The size-dependent behavior for composites at length-scales smaller than l_T has never before been the focus of investigation. For traditional rigid composites, the fracture behavior in the sub-l_T region cannot be studied through macroscopic mechanical tests, because in these materials l_T is extremely small (less than the mm-scale).[33-35] On the other hand, although traditional soft composites made from laminated rubbers can theoretically have very large l_T that implies the existence of a size-appropriate sub-l_T region, interfacial delamination between the matrix and fibers results in a separate failure mechanism, preventing this study.[36-39] Therefore, fiber-reinforced

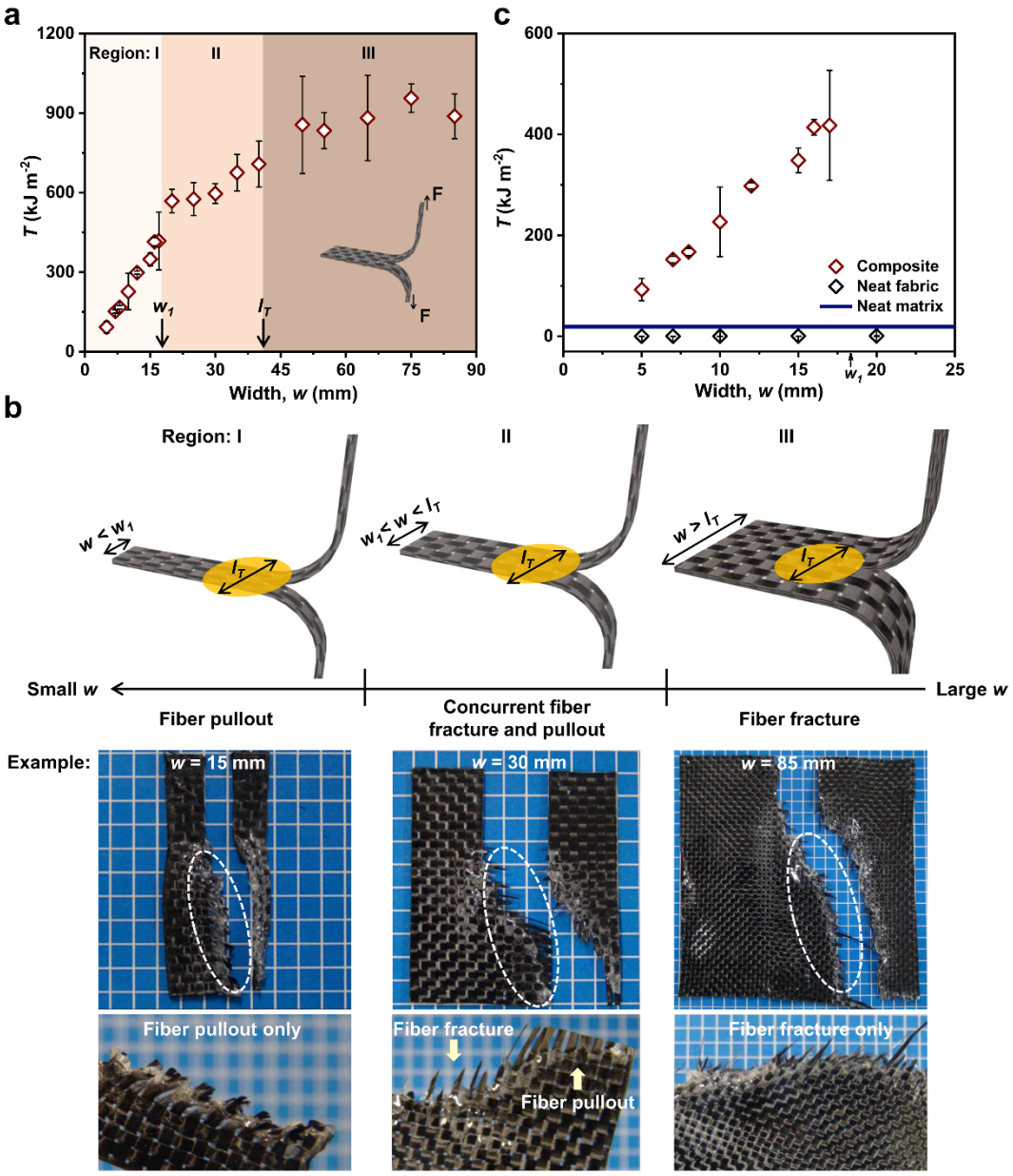

Figure 1. Size-dependent fracture behavior and toughness of soft FRPs. a) Toughness of the soft FRPs (M1-0.2/CF as an example, see **Figure S1** for the nomenclature of soft FRPs) with different widths. The composite toughness in this work is calculated using the fabric thickness (see **Figure S2** and related appendix in Supporting Information for details). When the sample is sufficiently large ($w > l_T$), the toughness is size-independent. When the specimen size is small ($w < l_T$), the toughness is size-dependent. b) Illustration and typical photo images of fractured composites in the three regions. In Region I ($w < w_1$) failure is due to fiber pullout and matrix rupture. Region II ($w_1 < w < l_T$) shows a mixed mode of fiber pullout and matrix/fiber concurrent failure. Region III ($w > l_T$) shows only matrix/fiber concurrent fracture. The white ellipses in b) are zoomed in to clearly indicate the areas where fiber fracture and fiber pullout occur. c) Enlarged plot highlighting Region I, where fracture only occurs by fiber pullout. The average toughness of the neat matrix and fabric in this Region is 19.0 and 0.4 kJ m^{-2}, respectively. Error bars represent standard deviation for $n \geq 3$ samples. The background grid size represents 5 mm.

viscoelastic polymers are uniquely qualified for investigating this region. Discerning the material and structural parameters governing the fracture mechanism in the sub-l_T region is of great significance and will facilitate the rational design and development of materials for use in size-limited applications that require high strength and crack resistance.[40, 41]

In this work, we establish a quantitative empirical relationship to show that the tearing toughness of soft composites, T, scales with the sample width, w, matrix toughness, T_m, and fiber bundle geometry factor, K. This relationship is based upon a simple fiber reinforced soft composites model with a perfect interface and can accurately calculate T for the limiting case that the soft composites fail through a single-mode fiber-pullout mechanism due solely to matrix fracture, with no fiber fracture or interfacial debonding. The relationship is proven experimentally for a variety of elastomers, fabrics, sample widths, and testing rates, with a total of 76 composite testing combinations. The results demonstrate that the presence of a stiff, reinforcing phase can result in significant toughness amplification when compared to a neat soft elastomer, even when both materials fracture solely through matrix rupture. We believe that the results of this study should give insight into the failure mechanism of other traditional FRPs in which l_T is too small to study the size-dependent fracture behavior experimentally. This work also provides a clear guide towards the future design of miniaturized soft materials devices by exploiting the benefits of FRPs at size-scales that have previously been ignored.

2. RESULTS

2.1. Microstructural Analysis of the Region I Soft FRPs

Viscoelastic matrices are synthesized through a copolymerization of ethylene glycol phenyl ether acrylate (PEA, M1) or 2-(2-phenoxyethoxy) ether acrylate (PDEA, M2) as a soft segment, and isobornyl acrylate (IBA) as a hard segment (**Figure S1**). Tensile and tearing mechanical properties of the matrices are shown in **Figure S3**, and **Figure S4**, respectively, and the results are summarized

in **Table S1**. Two types of carbon fiber fabrics with the same weave pattern but different fiber bundle geometries are used (**Figure S5**), which we refer to as thick carbon fiber (CF) and thin carbon fiber (t-CF) fabric, respectively. The structural parameters of the fabrics are summarized in **Table S2**. Soft FRPs made from different matrices and fabrics are coded as *x-f/y*, where *x* represents the soft segment chemistry, *f* represents the molar fraction of the hard segment, IBA, to the total monomer concentration, and *y* represents the type of fabric.

For each matrix and fabric combination, the occurrence of at least one fiber bundle fracture was the criterion for determining the transition point from Region I to Region II. This critical width is denoted as w_1, and the corresponding value for each sample is listed in **Table S3**. By utilizing the mechanical and structural parameters of the matrix and fiber bundle (**Figure S3**, **Figure S6**, and **Table S2**), we can also estimate w_1 through a force balance between the force applied to a single fiber bundle and the shear resistance by the surrounding matrix during fiber pullout (See **Figure S7a** and related appendix in Supporting Information for details). The experimental w_1 is plotted as a function of the theoretical w_1 in **Figure S7b**. The result shows that the experimental w_1 follows an empirical relationship:

$$w_{1,exp} = 0.76 w_{1,theo} = 0.76 \frac{\sigma_f A_f}{\sigma_m c} \quad (1)$$

where σ_f and σ_m are the fracture stress of a fiber bundle and the matrix, respectively, and A_f and c are the cross-sectional area and circumference of a fiber bundle, respectively. Note that a coefficient of 0.76 exists in the equation, indicating that the theoretical w_1 is overestimated. Because A_f and c are intrinsic geometry factors of a fiber bundle, we anticipate that the utilization of σ_f and σ_m obtained by testing individual components could be the source of the overestimation of theoretical w_1. The equation only considers a unidirectional fiber-reinforced soft composite, whereas the practical soft composites have a woven structure. σ_f is the tensile fracture stress of a neat fiber

bundle, however during the tearing of a soft composite, stress applied to the transverse fiber bundles exists in two directions: tensile stress is directly applied to the fiber bundle, along with perpendicular compressive stresses from the longitudinal fiber bundles. The additional compressive stress could lead to premature fracture. σ_m is the uniaxial tensile fracture stress of the neat matrix. However, during the tearing of a soft composite, the matrix experiences shear, rather than tensile deformation, since it is confined by the woven fiber structure. The practical fracture stress of the matrix could therefore also differ slightly. Since every parameter of the matrix and fiber bundle is measurable, we can estimate w_1 for any material combination using **Equation 1**, ensuring that all samples fall within Region I.

A composite sheet is formed when the monomers are synthesized in the presence of the carbon fiber fabric, as shown in the SEM images taken from a cross-section of an as-prepared M1-0.2/CF sample (**Figure 2**). Since fiber fracture does not occur at limited specimen size, it is important to explicitly demonstrate that the fibers and matrix are strongly adhered, which ensures effective load transfer. The cross-section was made by cutting the sample with scissors. As a control sample, we first examined the morphology of the two interlaced fiber bundles in a neat CF fabric without matrix. **Figure S8** shows that there is an obvious gap between the longitudinal (parallel to crack) and transverse (perpendicular to crack) fiber bundles, and that numerous voids exist within the longitudinal fiber bundle, providing space for the precursor monomer solution to enter. For the soft composite, the SEM observation shows two interwoven fiber bundles that are surrounded by matrix **(Figure 2a)**. A corresponding illustration is given in **Figure 2b** for clarity. Inside the longitudinal fiber bundle, individual fibers are encompassed by matrix (**Figure 2c**). The matrix also exists within the crossover region of the two perpendicularly aligned and interwoven fiber bundles (**Figure 2d**). The SEM observation reveals that the fibers are thoroughly imbedded in the soft

matrix to form strong bonding, owing to the good wettability of the precursor monomers onto the fabric.

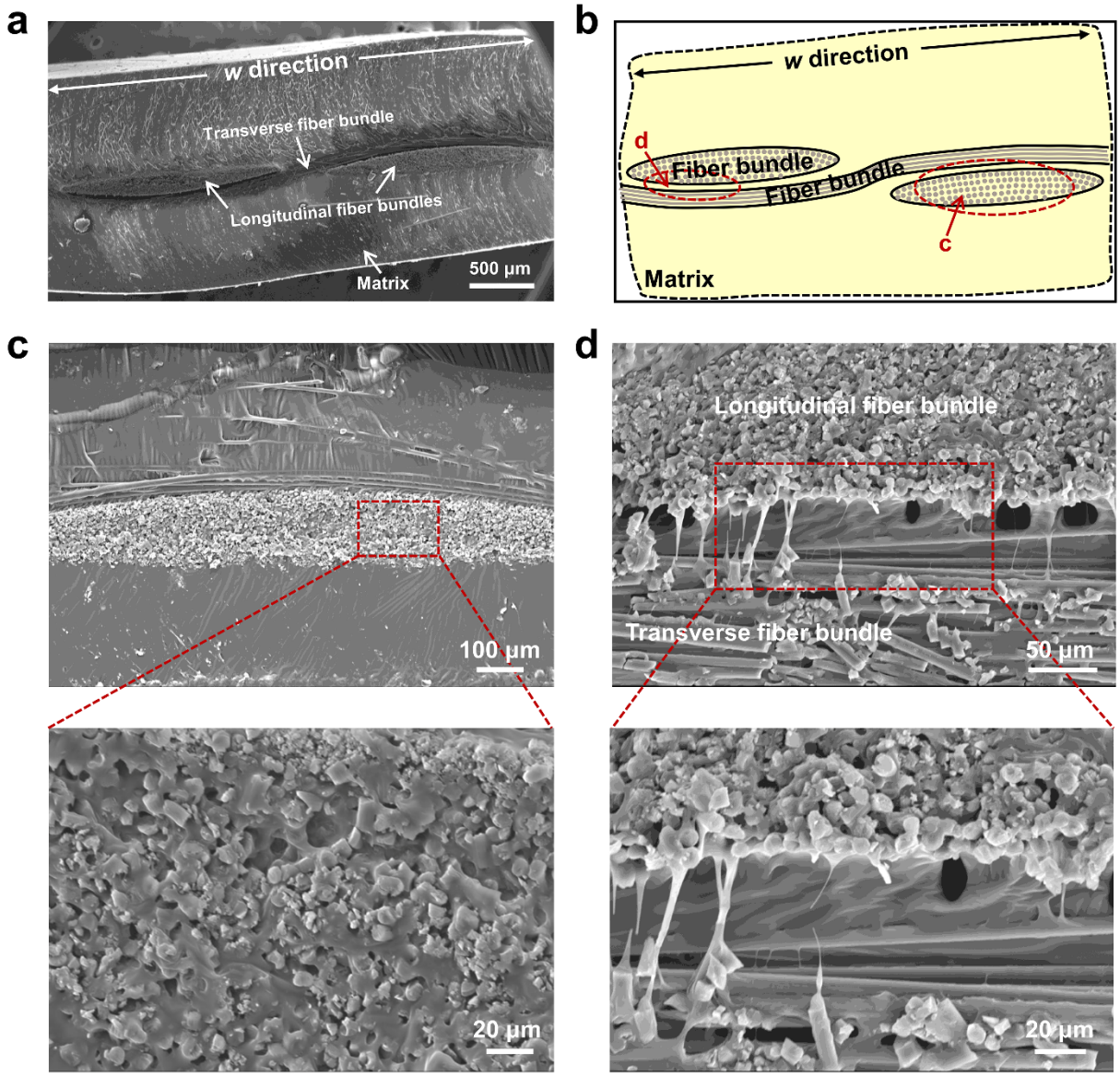

Figure 2. The microstructure of the soft FRPs by SEM observation. a) A cross-sectional view of the fiber bundles of the soft FRP made from P(PEA-co-IBA) (f=0.2) and thick carbon fiber fabric. (b) Corresponding illustration of the SEM image in (a). (c) SEM image of a longitudinal fiber bundle at the position "c" as shown in (b). Magnified image shows that individual fibers inside the fiber bundle are fully surrounded by the matrix. (d) SEM image of two interlaced fiber bundles at the position "d" shown in (b). Magnified image shows that the interlaced fiber bundles are connected by the matrix with some voids.

After confirming the structure and interface, we aimed to clarify the fracture mechanism for soft FRPs that exhibit only fiber pullout (Region I). The typical fiber-pullout failure behavior of a soft FRP before, during, and after a tearing test is shown in **Figure 3**. For the tearing test, the sample

was cut to the required geometry with a laser cutter. One leg was fixed to the bottom of the tensile tester, and the other leg was fixed to the crosshead with mechanical grips. Displacement was applied at 50 mm min^{-1} and the force was measured until the sample completely failed. The resulting force-displacement curve is shown in **Figure 3a**, and SEM images were taken at the crack tip region at different tearing times (**Figure 3b-d**). Before the test, the longitudinal fiber bundles appeared intimately connected with the transverse fiber bundle through matrix (**Figure 3b**). When the transverse fiber bundle undergoes pullout, the matrix existing within the crossover region becomes greatly deformed, resulting in prominent fibrillation (**Figure 3c**). Owing to the strong interface between components (resulting from two physical effects: van der Waals adhesion and topological interlocking),[20] cracks tend to be initiated in the matrix between the fiber bundles, rather than at the fiber-matrix interface, and propagate as fiber pullout proceeds. SEM images of a longitudinal and a transverse fiber bundle after pullout are shown in **Figure 3d (i)** and **(ii)**, respectively. The fiber bundles remain intact while the matrix between the bundles is fractured with residual matrix still bonded to the fiber bundle surface. The above results confirm that the fiber/matrix interface is strong and the failure behavior of the soft FRPs with $w < w_I$ is fiber-pullout-induced matrix rupture.

2.2. A simple model for understanding toughness in the fiber-pullout limit

Since the fracture behavior of soft FRPs in Region I is governed by fiber-pullout-induced matrix rupture and the fiber is much stiffer than the matrix, we can estimate the fracture energy (toughness) of the composites by only considering the energy dissipation of the matrix as:[19]

$$T = \frac{W\rho}{t} \, (w < w_I) \tag{2}$$

where W (J) is the energy required to pull out one transverse fiber bundle, ρ (m^{-1}) is the number of transverse fiber bundles per unit length in the soft FRPs, and t (m) is the relevant thickness. Samples fabricated with different matrix thicknesses showed no change in work to fracture, thus demonstrating that the fabric thickness is the relevant thickness (**Figure S2**). Because the energy dissipation stems from the fracture of matrix that has a fracture energy of T_m (J m^{-2}), W can be related to T_m roughly as $A \cdot T_m$, where A (m^2) is the fracture area of the matrix surrounding one fiber bundle. Assuming fracture occurs solely on the exterior of fiber bundles, the fracture area (A) of the matrix is equal to the circumference of the fiber bundle c, multiplied by the pullout length, which gives $\frac{cw}{2}$ (m^2). Note that the pullout length is $\frac{w}{2}$ since only a half-length of the transverse bundles is pulled out (**Figure 4**). Therefore, the energy required to pull out one fiber bundle is $T_m \cdot$

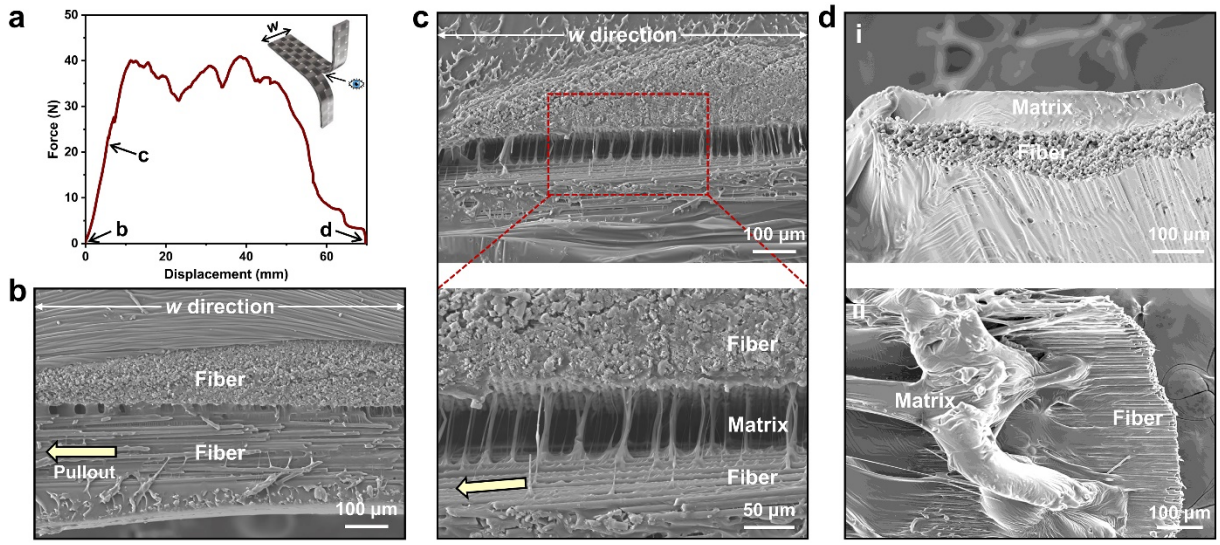

Figure 3. The fiber-pullout fracture behavior of the soft FRPs around the crack tip. a) Force-displacement curve of the tearing test of the soft FRP (w = 10 mm). The b, c, d denoted on the curve correspond to the figures (b), (c), and (d), respectively. The first peak of this curve indicates the onset of fiber pullout. b) SEM image of two interlaced fiber bundles in the original soft FRP before loading at point b. c) SEM image and corresponding magnified region of two interlaced fiber bundles during deformation at point c. Significant fibrillation of the matrix is observed in the interlaced region, which accounts for large energy dissipation. d) SEM images of a longitudinal (i) and a transverse (ii) fiber bundle after pullout at point d. The fractured matrix remains adhered to the fiber bundles, indicating strong bonding at the fiber/matrix interface.

$A = T_m \cdot \frac{cw}{2}$ (J). Consequently, the energy of fiber pullout (i.e., the energy to fracture the soft FRP) by matrix rupture per unit area of the soft FRP in Region I should be $\frac{cw}{2} T_m \frac{\rho}{t}$ (J m^{-2}). A simplified form is given as:[35]

$$T \cong KT_m w \ (w < w_1) \quad (3)$$

where the parameter $K = \frac{c\rho}{2t}$ is termed the fiber bundle geometry factor. For a composite with a center-to-center distance between adjacent fiber bundles, w_{cc} and fabric thickness, t, $\rho = \frac{1}{w_{cc}}$ (See **Figure S9** and related appendix for the calculation of ρ), so $K = \frac{c}{2tw_{cc}}$ (**Figure 4**). The fibers are much stiffer than the soft matrix, and do not deform significantly during pullout. Therefore, the mechanical response of the fibers is not explicitly included in **Equation 3**. We will use this equation as a guide to systematically explore how each variable influences T.

2.3. Experimental Investigation

To investigate the suitability of **Equation 3**, we performed two series of experiments: 1) soft FRPs were made from the same matrix (fixed T_m) but different fabrics to investigate the relationship

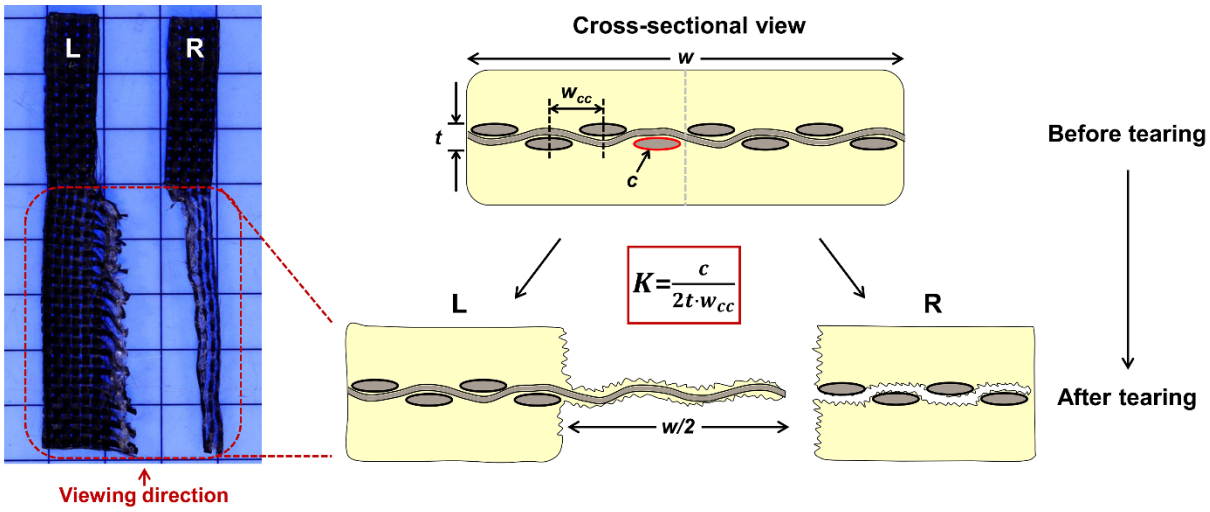

Figure 4. Photograph and illustration of two halves (left and right) of a soft FRP after tearing with w = 10 mm. Fiber-pullout occurs, and the transverse fiber bundles remain in one half of the sample, shown by the left (L) sample in the photograph and illustration. Crack initiation and propagation occurs through the matrix. The fiber pullout length is equal to $w/2$. The background grid size is 5 mm.

between T and K at different w; and 2) soft FRPs were made from the same fabric (fixed K) but different matrices to investigate the relationship between T and T_m at different w. From these results, we can understand the w-dependence of T for different K and T_m.

First, the effect of fiber bundle geometry factor (K) on the toughness of soft FRPs is investigated. Composite samples are made with M1-0.25 as the matrix and have a width within Region I (w = 7 mm) to ensure the soft FRPs fail via single-mode fiber pullout (**Table S3**). Both CF and t-CF fabrics are utilized, which have K of 3070 m^{-1} (CF) and 5310 m^{-1} (t-CF), respectively. Note that K represents the ratio of the perimeter length of fiber bundles to cross-sectional area of a composite, and thus higher K results in more surface area per volume of fabric. The tearing tests were performed at a velocity of 50 mm min^{-1}. The force versus displacement curves during tearing for the M1-0.25/CF and M1-0.25/t-CF samples with w = 7 mm can be seen in **Figure 5a** as the black and blue curves, respectively. Composite toughness, T, can be obtained by integrating the force versus displacement curves and then dividing by the cross-sectional area of fractured composite (**Experimental Section**). The soft composite prepared from t-CF exhibits higher tearing force and fracture toughness compared to the CF reinforced composite, although both composites contain the same matrix. Even without fiber fracture, the presence of the fabric influences the toughening mechanism. The role of matrix toughness (T_m) on composite toughness (T) for various w in Region I was subsequently investigated. For this purpose, the fabric is fixed as CF, while the matrix properties are varied. A third sample with higher T_m than M1-0.25 was introduced (M2-0.5/CF) as the red curve in **Figure 5a** and can be compared to the M1-0.25/CF sample from above. Similar to the fabric effect, we observe that at the same width, modifying the toughness of the matrix influences the force of the tearing curves, which consequently results in different T. Similar results are obtained by adjusting the testing velocity for a specific composite composition. Since the matrix used in this work is highly viscoelastic, the T_m can be tuned by adjusting the testing velocity (**Figure**

S4, **Table S1**). As another example shown in **Figure S10**, the toughness of the M1-0.1/CF composite with a width of 10 mm increases with testing velocity, proving that the matrix toughness has a significant effect on the composite toughness. These results are also in agreement with our previous work for soft composites made from hydrogels, which demonstrates that the toughness of hydrogel composites with fixed width increases with increasing T_m.[18]

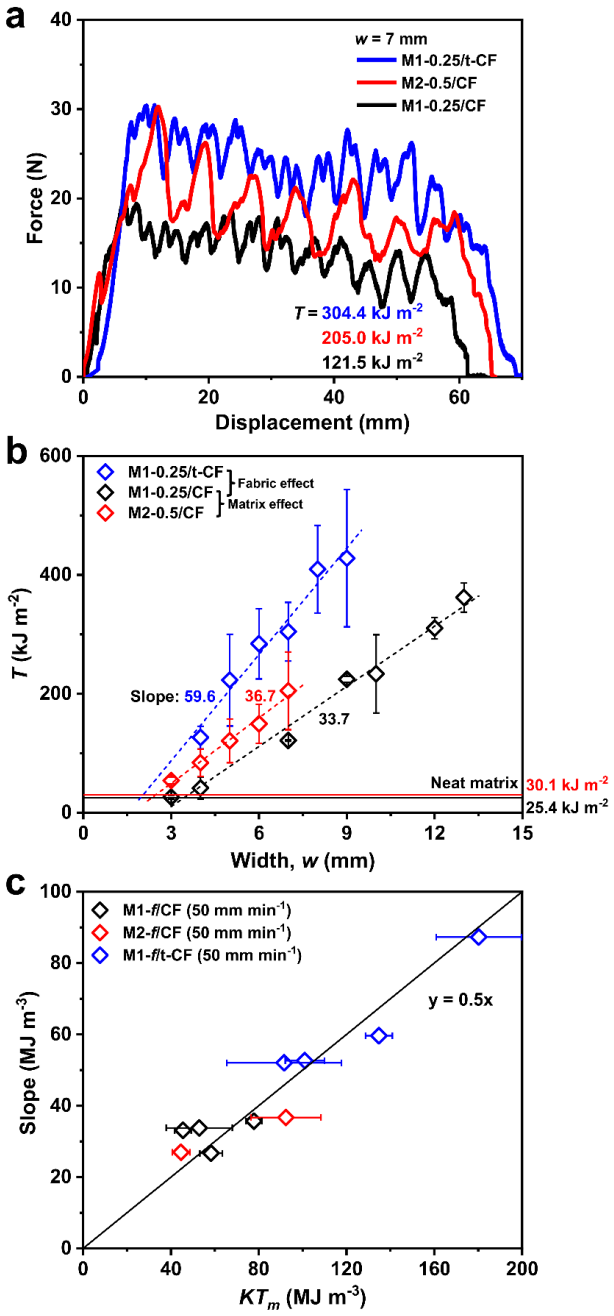

Figure 5. Factors influencing the toughness, *T*, of soft FRPs. a) Force-displacement curves of soft FRPs

(w = 7 mm) made from varied CF fabrics or matrices. The testing velocity of the tearing test was 50 mm min^{-1}. b) Tearing energy (toughness), T, of the soft FRPs made from varied CF fabrics or varied matrices, versus sample width, w. The horizontal red and black lines represent the toughness of neat matrix M2-0.5 and M1-0.25, respectively. c) The slope of the relationship $T \sim w$ (from b), versus KT_m (measured from components) for different combinations and testing velocities of soft composites. Error bars represent standard deviation for n ⩾ 3 samples. The results of curve-fitting to tested data in (b) and (c) are summarized in **Table S4**.

For each sample configuration introduced above, numerous sample widths were tested within Region I. **Figure 5b** shows a linear plot of T as a function of w for these three sets of soft composites. For each data point, n⩾3 specimens were tested to obtain the average value and standard deviation. Linear regressions of these data (dashed lines) show a good fit, with R^2 values of 0.964 (blue), 0.985 (red), and 0.987 (black) (**Table S4**). The curve-fitting results reveal a linear relationship between T and w for each sample combination, acting to confirm the relationship expressed in **Equation 3**. Two interesting results are observed. First, the intercepts for all fits are negative, rather than passing through the origin. This finding indicates that there should be a lower bound of T for soft FRPs when the sample width is sufficiently small. We anticipate that when the sample width of soft FRPs is too small, the role of the fabric to transfer the load no longer influences T significantly. In this case, the soft FRP fracture process is similar to merely rupturing the neat matrix. Therefore, T_m is expected to be the lower bound of T for the soft FRPs with considerably small width. The values of T_m for the two different matrices are plotted as horizontal lines in **Figure 5b**. The M1-0.25/CF composite with w = 3 mm reaches nearly $T = T_m$, and extrapolation of the trend lines for the other samples show an intersection with T_m at similar w, supporting our hypothesis. We consider that for very small samples, at least two partial longitudinal bundles should exist for fiber pullout to occur. Therefore, we expect Region I to have a minimum bound at a width equal to the center-to-center distance between adjacent fiber bundles, w_{cc}. Based on this result, we modify **Equation 3** as

$$T_c \cong KT_m(w - w_{cc}) + T_m \quad (w_{cc} < w < w_1) \tag{4}$$

CF and t-CF have w_{cc} of 2.07 and 1.32 mm, respectively, which agrees well with the intercept points shown in **Figure 5b**. Based on the above considerations, w_{cc} will be considered the lower bound of Region I, and we will focus our remaining experiments on w that falls within the fiber-pullout region ($w_{cc} < w < w_1$).

The second interesting result of **Figure 5b** is that the slope for the linear relationship, $T \sim w$, of each combination differs, indicating that both fabric geometry and matrix toughness play important roles in controlling the composite toughness. Based on **Equation 4**, the slope for the linear relationship, $T \sim w$, should be KT_m. To verify this, we obtained the values of the slopes from the linear regressions of the experimental data (for each data point, n⩾3 specimens were tested to obtain the average value and standard deviation) for a total of ten different materials combinations made from six types of matrices and two types of fabrics (**Figure S11**) and plotted them as a function of KT_m as measured from the individual components in **Figure 5c**. The linear regression exhibits a good fit with an R^2 value of 0.981 (**Table S4**), indicating that the slope is linearly

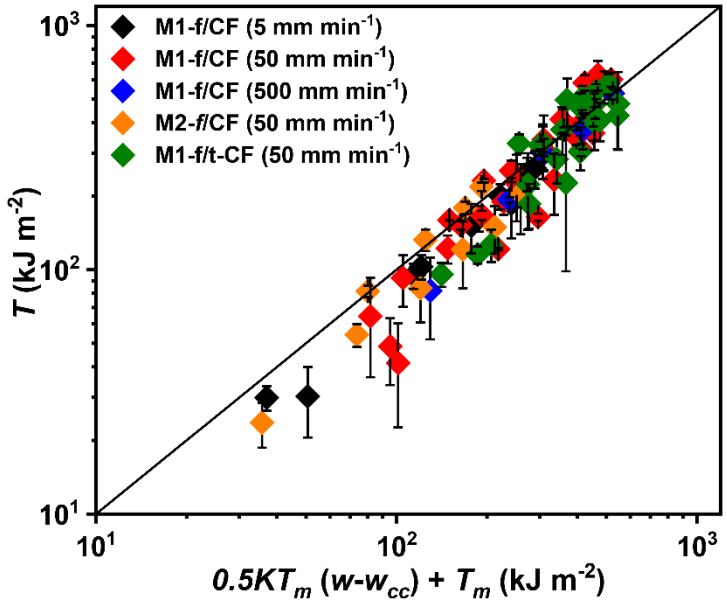

Figure 6. An empirical law to predict the composite toughness from component parameters. Over nearly two orders of magnitude, a good agreement between the experimental data and the semi-empirical equation for the composite toughness is observed. The solid line is the prediction according to **Equation 5**. Error bars represent standard deviation for n ⩾ 3 specimen.

proportional to KT_m with a proportionality coefficient of 0.5. Thus, we get a semi-empirical relationship:

$$T = 0.5KT_m(w - w_{cc}) + T_m \qquad (w_{cc} < w < w_1) \tag{5}$$

Finally, we tested whether **Equation 5** can be applied universally to describe the fracture toughness of all soft FRPs in the width-dependent fiber-pullout region ($w_{cc} < w < w_1$). In total, 76 composite combinations, with a total sample size of $n = 248$ of various K, T_m, w, and testing velocity were measured. For each data point, n⩾3 specimens were tested to obtain the average value and standard deviation. **Figure 6** plots the experimental fracture energy (T) of all soft FRPs as a function of the quantity $0.5KT_m(w\text{-}w_{cc}) + T_m$. Over two orders of magnitude, the experimental values of T follow the linear scaling relation of **Equation 5**, further validating the semi-empirical relationship. The above results indicate that matrix toughness, fiber bundle geometry factor, and sample width are the parameters that act to scale toughness of soft FRPs when failure occurs without fiber fracture.

The good fit observed in **Figure 6** demonstrates that without any fitting parameter, we can calculate the fracture toughness of soft FRPs for Region I. There are a few potential reasons why a coefficient of 0.5 appears in **Equation 5**. First of all, 2D woven fabrics are very complex, and our analysis is based upon a simplified 1D fiber pull-out model, like in other previous attempts.[34, 35] During testing, significant twisting and distortion of the sample occurs during the failure process (**Movie S1**). Twisting during failure could result in a slower pullout velocity of the fiber bundles from the matrix. In this case, T_m would decrease due to decreased deformation rate, leading to overestimation of T. Furthermore, T_m was calculated by a Mode III tearing test of the neat elastomers, while the fracture process between fiber bundles likely initiates by a Mode II shear deformation. Even so, utilizing a constant coefficient of 0.5 results in a simplified model that quantitatively describes the fracture energy for many different material combinations and testing

conditions.

Note that in **Equation 5** we assume that energy is dissipated solely by fracture of matrix surrounding the fiber bundles, and fracture of the matrix along the crack path is ignored. For samples of a width w far above w_{cc}, fracture of the elastomer matrix in the crack region accounts for less than 10% of the fiber-pullout work, but as the specimen size decreases and w approaches w_{cc}, this term increases up to ~45% (**Figure S12**). To summarize, from **Equation 5** one can predict the toughness of soft FRPs with high precision in the absence of fiber fracture using geometry parameters of fabric $K = \frac{c}{2tw_{cc}}$ and the toughness T_m of the matrix determined experimentally.

3. DISCUSSION

A simple rearrangement of **Equation 5** allows us to directly study the impact that the fabric has on the composite. We define η as the toughness amplification factor, which describes the relative increase in toughness of the composite compared to the neat matrix:

$$\eta = \frac{T}{T_m} - 1 = 0.5K(w - w_{cc}) \quad (6)$$

Since both K and w_{cc} are directly defined by the characteristics of the fabric, we can isolate the fabric contribution. A plot of η versus (w - w_{cc}) is shown in **Figure 7**. We can see that for the materials fabricated in this work, we can achieve η up to a factor of ~41, demonstrating a clear synergistic increase in toughness. The toughness amplification factor scales with w, while the slope of the relation (linear regression with R^2 values of 0.962 (black), 0.965 (red), as shown in **Table S4**) changes for different fabrics due to variations in K. This result means that for samples of the same width, a larger geometric factor, K, results in stronger toughness amplification. $K = \frac{c}{2tw_{cc}}$ is determined by the ratio of the perimeter length (c) of a bundle and the cross-sectional area of the crack that contains one fiber bundle, $t \cdot w_{cc}$. These two terms are related, and thus a change in fiber bundle shape is required to substantially change K. In comparing the two fabrics tested here, the

cross-sectional area of the t-CF bundles is only 30% of the CF bundles, yet they possess 55% of the perimeter length. Such a synergy generates a higher K for the t-CF. These results show that the geometric parameters making up the fabric plays an important role in determining the degree of toughness enhancement, even though the fibers do not contribute to the energy dissipation through fracture.

Within the fiber-pullout limits discussed here, fracture occurs only within the matrix. Despite not directly rupturing to dissipate energy, the presence of fibers dramatically increases the toughness of these soft FRPs. Generally, such a soft matrix itself can only dissipate energy in a highly limited zone because its intrinsic load transfer length is on the scale of hundreds of microns.[20, 33, 42-44] Through the incorporation of a stiff woven fabric, we have modified the neat elastomer to include a reinforcing foundation that at the sample scale investigated here cannot fracture, but can move, significantly increasing the load transfer length. During tearing the viscoelastic matrix experiences large deformation and the fibrillation at the interlaced region might

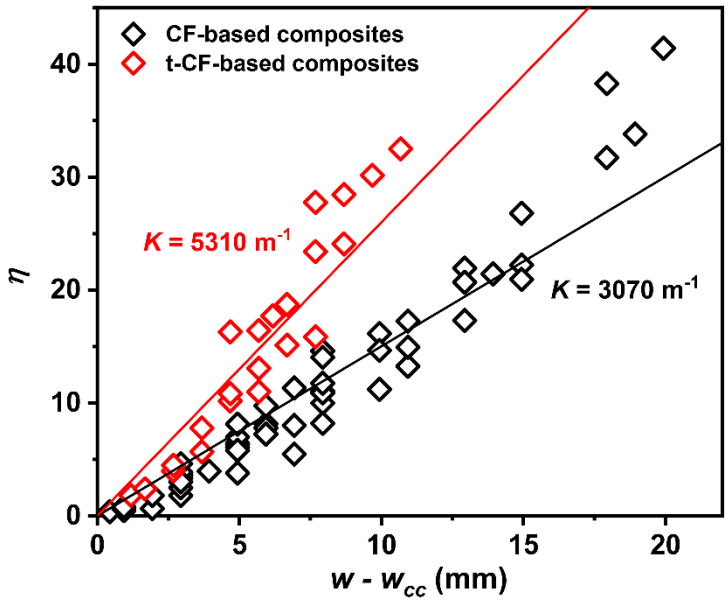

Figure 7. The toughness amplification factor (η) of all soft FRPs as a function of composite width, w. The result shows that the toughness amplification factor scales with w, while the slope of the relation is dominated by the fiber bundle geometry factor (K) of different fabrics. The results of curve-fitting of the tested data are shown in **Table S4**.

dissipate large amount of energy. To fracture the sample, the crack must propagate around the cylindrical plane of each bundle undergoing pullout due to the strong fiber/matrix interface, running perpendicular to the nominal fracture plane. The rigid/soft combination enables the force to be transferred along the entire sample width, giving rise to a greatly improved energy dissipation zone. This significant modification of the matrix fracture plane from a 2D-straight path to a 3D-serpentine path results in the high toughness amplification factor seen here.

The establishment of the quantitative relationship shown by **Equation 5** gives a design principle for tough, soft FRPs at considerably limited sizes when fracture is governed solely by fiber pullout. For an application utilizing soft composites that has explicit requirements of fracture toughness and specimen size, an engineer or manufacturer can easily balance the matrix properties and fabric geometry according to **Equation 5**. Depending on the situation, the designer can either first determine a suitable matrix (with appropriate bending stiffness, for example) and then select the reinforcing fabric (based on tensile strength and fiber bundle geometry factor) that will provide sufficient toughness. On the other hand, if the application merely stipulates the specimen size, then the fracture toughness can be optimized by maximizing the fiber bundle geometry factor and utilizing high-toughness matrices. As an example, we show that combining a tough matrix poly(PEA-co-IBA) (M1-0.15, T_m=17.3 kJ m^{-2}) with a thin carbon fiber (t-CF) fabric that possesses large K (5.3×10^3 m^{-1}) enables a size-limited soft FRP (width = 10 mm) to achieve a high tearing toughness of over 500 kJ m^{-2} (**Table S3**). Due to the high in-plane stiffness of carbon fiber, these materials possess very high tensile modulus, yet are extremely flexible and soft to the touch. This unique combination of contrasting properties makes them especially suitable for advanced soft materials devices currently being developed.

Also, note that Region II from $w_1 < w < l_T$ (**Figure 1c**) is width-sensitive. In this region, toughness is initially governed by fiber fracture that transforms into fiber pullout after a certain

number of fibers are broken. This mixed-mode fracture process is not well described by either the fiber-pullout model in this work or our preceding fiber-fracture model. We expect that this region can be modeled through a serial combination of both fracture mechanisms, and we will investigate this mixed-mode region in future work.

4. CONCLUSION

In this work, we empirically describe the fracture toughness of soft FRPs made from a combination of viscoelastic polymers and fabrics at limited size scales where the failure process is governed by a single-mode fiber pullout mechanism by matrix fracture. With the aid of a simple fiber-pullout model, we demonstrate that three parameters control the toughness (T) of soft FRPs that fail by fiber pullout: matrix toughness (T_m), fiber bundle geometry factor (K), and the size of the composite (w). To generate FRPs with high toughness at a fixed small width, both the fiber bundle geometry factor and the matrix toughness should be maximized. Based on this strategy, we show how soft FRPs with limited size can reach unprecedented levels of crack resistance. This study clarifies the energy dissipation mechanism of soft FRPs in the pullout limit and introduces a general principle to maximize the fracture toughness of soft FRPs at small length scales, which can guide the design of extremely tough yet size limited soft FRPs in industrial applications.

5. EXPERIMENTAL PROCEDURES

Materials: Plain weave carbon fiber fabric (CF) and thin carbon fiber fabric (t-CF) were purchased from Marukatsu Co., Ltd., Japan. Both fabrics were used as received. The textures and geometric parameters of the fabrics are given in **Figure S5** and **Table S2**, respectively. Acrylate monomers, ethylene glycol phenyl ether acrylate (PEA), 2-(2-phenoxyethoxy)ether acrylate (PDEA), and isobornyl acrylate (IBA) were provided by Osaka Organic Chemical Industry Ltd, Japan. Ultraviolet initiator benzophenone (BP) was purchased from KANTO Chemical Co., Inc and used without further purification.

Fabrication of soft fiber-reinforced polymers (soft FRPs): Samples were prepared by placing two spacers with a thickness of 0.5 mm on both sides of the fabric, which was inserted between two hydrophobic films supported by glass plates to form a reaction mold. Subsequently two monomers, one of ethylene glycol phenyl ether acrylate (PEA) or 2-(2-phenoxyethoxy) ether acrylate (PDEA), along with isobornyl acrylate (IBA), containing initiator (0.1 mol% of the total monomer molar concentration) was injected into the mold.[45] Random copolymerization was allowed to proceed under an argon atmosphere via ultraviolet irradiation (UVP lamp Toshiba-FL15BLB, wavelength 365 nm, light intensity 4 mW cm^{-2}) for 10 h.

Uniaxial tensile tests: Tensile tests on neat matrices were conducted using a tensile tester (Autograph AG-X, Shimadzu Co., Japan) equipped with a 100 N load cell at room temperature in air. Before the tests, the matrices were cut into a dumbbell shape standardized as JIS-K6251-7 (2 mm in inner width, 12 mm in gauge length) with a cutting machine (Dumb Bell Co., Ltd.). The tensile strain rates varied from 0.007, 0.07, to 0.7 s^{-1}, corresponding to testing velocities of 5, 50, and 500 mm min^{-1}.

Trouser tearing tests: Trouser tearing tests were used to measure the tearing fracture energy of soft FRPs. The tests were performed using a tensile tester (Autograph AG-X, Shimadzu Co., Japan) equipped with a 20 kN load cell. Samples with a width, w, smaller than 30 mm were prepared with a length of 50 mm. Samples with a width larger than 30 mm were prepared with a length of $w + 20$ mm. An initial notch of 20 mm was made in the middle of the sample along the length direction with a laser cutter. For comparison, neat CF fabric was tested under the same experimental condition with the soft FRPs. Neat viscoelastic polymers are also tested. Samples were prepared with a prescribed width, w, and length of 50 mm. Also, an initial notch of 20 mm was made in the middle of the sample along the length direction with a laser cutter. To prevent elongation of the legs of polymers during tests, stiff and thin tape was glued on both sides of the samples prior to

tests. During testing, one leg of the sample was clamped to the base, and the other was clamped to the crosshead, which was displaced at a velocity of 5, 50, or 500 mm min^{-1} at room temperature in the open atmosphere. After testing, the tearing force-displacement curves were obtained to calculate the tearing energy of samples by the following equation:[10, 17-19, 46, 47]

$$T = \frac{\int_0^L F\, dL}{t \cdot L_{bulk}} \tag{7}$$

where F is the tearing force, t is the fabric thickness for the soft composites or the matrix thickness for the neat matrix, L is the displacement, and L_{bulk} is the projected crack length.

Scanning electron microscopy: Microscale observation was carried out by scanning electron microscopy (SEM) (JEOL JSM-6010LA, Tokyo, Japan). Samples were gold-coated in an ion-sputtering machine (E-1010, Hitachi, Tokyo, Japan) before observation. The acceleration voltage varied from 15 to 20 kV.

SUPPLEMENTAL INFORMATION

Supplemental Information can be found online at

ACKNOWLEDGEMENTS

This research was financially supported by Grant-in-Aid for Scientific Research Nos. 17H06144 and 20K20193. The Institute for Chemical Reaction Design and Discovery (ICReDD) was established by World Premier International Research Initiative (WPI), MEXT, Japan. C.Y. Hui is supported by the National Science Foundation, under Grant No. CMMI-1903308.

AUTHOR CONTRIBUTIONS

Conceptualization, W.C., D.R.K., and J.P.G.; Methodology, W.C., Y.H., L.C., Y.S., Y.Z., and T.K.; Investigation, W.C., Y.H., L.C., Y.S., and Y.Z.; Writing-Original Draft, W.C; Writing-Review & Editing, W.C., C.-Y.H., D.R.K., and J.P.G.; Supervision, D.R.K. and J.P.G.; Funding Acquisition, C.-Y.H., D.R.K., and J.P.G.

DECLARATION OF INTERESTS

The authors declare no competing interests.

REFERENCES

[1] J. P. Gong, Y. Katsuyama, T. Kurokawa, Y. Osada, *Adv. Mater.* **2003**, 15, 1155.
[2] J. P. Gong, *Soft Matter* **2010**, 6, 2583.
[3] J.-Y. Sun, X. Zhao, W. R. Illeperuma, O. Chaudhuri, K. H. Oh, D. J. Mooney, J. J. Vlassak, Z. Suo, *Nature* **2012**, 489, 133.
[4] T. L. Sun, T. Kurokawa, S. Kuroda, A. B. Ihsan, T. Akasaki, K. Sato, M. A. Haque, T. Nakajima, J. P. Gong, *Nat. Mater.* **2013**, 12, 932.
[5] E. Ducrot, Y. Chen, M. Bulters, R. P. Sijbesma, C. Creton, *Science* **2014**, 344, 186.
[6] K. Haraguchi, T. Takehisa, *Adv. Mater.* **2002**, 14, 1120.
[7] Z. Wang, C. Xiang, X. Yao, P. Le Floch, J. Mendez, Z. Suo, *Proc. Natl. Acad. Sci. USA* **2019**, 116, 5967.
[8] E. J. Markvicka, M. D. Bartlett, X. Huang, C. Majidi, *Nat. Mater.* **2018**, 17, 618.
[9] R. Takahashi, T. L. Sun, Y. Saruwatari, T. Kurokawa, D. R. King, J. P. Gong, *Adv. Mater.* **2018**, 30, 1706885.
[10] A. M. Hubbard, W. Cui, Y. Huang, R. Takahashi, M. D. Dickey, J. Genzer, D. R. King, J. P. Gong, *Matter* **2019**, 1, 674.
[11] S. Lin, C. Cao, Q. Wang, M. Gonzalez, J. E. Dolbow, X. Zhao, *Soft Matter* **2014**, 10, 7519.
[12] A. Agrawal, N. Rahbar, P. D. Calvert, *Acta Biomater.* **2013**, 9, 5313.
[13] D. Zhalmuratova, H. J. Chung, *ACS Appl. Polym. Mater.* **2020**, 2, 1073.
[14] I. C. Liao, F. T. Moutos, B. T. Estes, X. Zhao, F. Guilak, *Adv. Funct. Mater.* **2013**, 23, 5833.
[15] A. N. Gent, J. D. Walter, The pheumatic tire, **2006**.
[16] X. Yang, Z. Zhang, J. Yang, Y. Sun, *SpringerPlus* **2016**, 5, 1573.
[17] D. R. King, T. L. Sun, Y. Huang, T. Kurokawa, T. Nonoyama, A. J. Crosby, J. P. Gong, *Mater. Horiz.* **2015**, 2, 584.
[18] Y. Huang, D. R. King, T. L. Sun, T. Nonoyama, T. Kurokawa, T. Nakajima, J. P. Gong, *Adv. Funct. Mater.* **2017**, 27, 1605350.
[19] Y. Huang, D. R. King, W. Cui, T. L. Sun, H. Guo, T. Kurokawa, H. R. Brown, C.-Y. Hui, J. P. Gong, *J. Mater. Chem. A* **2019**, 7, 13431.
[20] W. Cui, D. R. King, Y. Huang, L. Chen, T. L. Sun, Y. Guo, Y. Saruwatari, C. Y. Hui, T. Kurokawa, J. P. Gong, *Adv. Mater.* **2020**, 32, 1907180.
[21] D. C. Hofmann, J.-Y. Suh, A. Wiest, G. Duan, M.-L. Lind, M. D. Demetriou, W. L. Johnson, *Nature* **2008**, 451, 1085.
[22] L.-B. Mao, H.-L. Gao, H.-B. Yao, L. Liu, H. Cölfen, G. Liu, S.-M. Chen, S.-K. Li, Y.-X. Yan, Y.-Y. Liu, *Science* **2016**, 354, 107.
[23] L. Xu, X. Zhao, C. Xu, N. A. Kotov, *Adv. Mater.* **2018**, 30, 1703343.
[24] M. D. Demetriou, M. E. Launey, G. Garrett, J. P. Schramm, D. C. Hofmann, W. L. Johnson, R. O. Ritchie, *Nat. Mater.* **2011**, 10, 123.
[25] B. L. Smith, T. E. Schäffer, M. Viani, J. B. Thompson, N. A. Frederick, J. Kindt, A. Belcher, G. D. Stucky, D. E. Morse, P. K. Hansma, *Nature* **1999**, 399, 761.
[26] E. Munch, M. E. Launey, D. H. Alsem, E. Saiz, A. P. Tomsia, R. O. Ritchie, *Science* **2008**, 322, 1516.
[27] G. Lake, A. Thomas, *Proc. R. Soc. London A* **1967**, 300, 108.

[28] K. Volokh, P. Trapper, *J. Mech. Phys. Solids* **2008**, 56, 2459.
[29] J. M. Hedgepeth, **1961**.
[30] H. Cox, *Br. J. Appl. Phys.* **1952**, 3, 72.
[31] M. F. Ashby, D. Cebon, *Le Journal de Physique IV* **1993**, 3, C7.
[32] B. Gludovatz, A. Hohenwarter, D. Catoor, E. H. Chang, E. P. George, R. O. Ritchie, *Science* **2014**, 345, 1153.
[33] C. Chen, Z. Wang, Z. Suo, *Extreme Mech. Lett.* **2017**, 10, 50.
[34] C.-Y. Hui, Z. Liu, S. L. Phoenix, *Extreme Mech. Lett.* **2019**, 33, 100573.
[35] C.-Y. Hui, Z. Liu, S. L. Phoenix, D. R. King, W. Cui, Y. Huang, J. P. Gong, *Extreme Mech. Lett.* **2020**, 100642.
[36] R. Pan, D. Wati, *Polym. Compos.* **1996**, 17, 486.
[37] M. Mehan, L. Schadler, *Compos. Sci. Technol.* **2000**, 60, 1013.
[38] Q. Meng, M. Chang, *Int. J. Solids Struct.* **2020**, 188, 141.
[39] W. R. Illeperuma, J.-Y. Sun, Z. Suo, J. J. Vlassak, *Extreme Mech. Lett.* **2014**, 1, 90.
[40] R. F. Shepherd, A. A. Stokes, R. M. Nunes, G. M. Whitesides, *Adv. Mater.* **2013**, 25, 6709.
[41] S. Keten, Z. Xu, B. Ihle, M. J. Buehler, *Nat. Mater.* **2010**, 9, 359.
[42] R. Bai, B. Chen, J. Yang, Z. Suo, *J. Mech. Phys. Solids* **2019**, 125, 749.
[43] J. Liu, C. Yang, T. Yin, Z. Wang, S. Qu, Z. Suo, *J. Mech. Phys. Solids* **2019**, 133, 103737.
[44] R. Long, C. Y. Hui, J. P. Gong, E. Bouchbinder, *Annu. Rev. Condens. Matter Phys.* **2021**, 12, 71.
[45] L. Chen, T. L. Sun, K. Cui, D. R. King, T. Kurokawa, Y. Saruwatari, J. P. Gong, *J. Mater. Chem. A* **2019**, 7, 17334.
[46] E. Triki, P. Dolez, T. Vu-Khanh, *Compos. Part B Eng.* **2011**, 42, 1851.
[47] E. Triki, T. Vu-Khanh, P. Nguyen-Tri, H. Boukehili, *Theor. Appl. Fract. Mec.* **2012**, 61, 33.